J Mater Sci

Metals

The shock-induced chemical reaction behaviour of Al/Ni composites by cold rolling and powder compaction

Wei Xiong[1], Xianfeng Zhang[1,*], Li Zheng[2], Kuo Bao[1], Haihua Chen[1], and Zhongwei Guan[3]

[1] *School of Mechanical Engineering, Nanjing University of Science and Technology, Xiaolingwei 200, Nanjing 210094, China*
[2] *School of Material Science and Engineering, Shenyang University of Technology, Shenliao West Road 111, Economic and Technological Development Zone, Shenyang 110870, China*
[3] *School of Engineering, University of Liverpool, Brownlow Street, Liverpool L69 3GQ, UK*

Received: 5 October 2018
Accepted: 15 January 2019

ABSTRACT

Al/Ni composites are typical structural energetic materials, which have dual functions of structural and energetic characteristics. In order to investigate the influence of manufacturing methods on shock-induced chemical reaction (SICR) behaviour of Al/Ni composites, Al/Ni multi-layered composites with 3–5 cold-rolling passes and Al/Ni powder composites were obtained. Microstructural observation using scanning electron microscopy (SEM) and two-step impact initiation experiments were performed on the four Al/Ni composites. Furthermore, mesoscale simulations, through importing SEM images into the finite element analysis to reflect the real microstructures of the composites, were performed to analyse the particle deformation and temperature rise under shock compression conditions. The experimental results showed the distinct differences on the SICR characteristics among the four Al/Ni composites (i.e. by 3, 4 and 5 cold-rolling passes and powder compaction). The manufacturing methods provided the control of the particle sizes, particle distribution and the content of the interfacial intermetallics at scale of different microstructures, which ultimately affected the temperature distribution, as well as the contact between Al and Ni in Al/Ni composites under shock loading. As a result, the Al/Ni powder composites showed the highest energy release capacity among the four composites, while the energy release capability of Al/Ni multi-layered composites decreased with the growth of rolling passes.

A1 A2 Address correspondence to E-mail: lynx@njust.edu.cn

https://doi.org/10.1007/s10853-019-03357-3

Springer

Journal : 10853 - Large 10853 | Dispatch : 17-1-2019 | Pages : 17
Article No. : 3357 | LE | TYPESET
MS Code : JMSC-D-18-08395 | CP | DISK

Introduction

Al/Ni composites have advantages of low density, high melting point and high strength-to-weight ratio, as well as high energy release capability, which can produce different reaction products such as $NiAl_3$, NiAl, Ni_2Al_3 and Ni_3Al at various temperatures and shock compression conditions [1, 2]. Al/Ni composites belong to energetic structural materials (ESMs), which have many potential applications such as reactive shaped charge liner, reactive material projectile and reactive fragmentation [3–5], due to their dual functionality. In such applications, chemical reaction is initiated in the ESMs under shock conditions, which is commonly called shock-induced chemical reaction (SICR). Extensive impact experiments [6, 7] revealed that the microstructures, including particle sizes, shapes and distributions, have significant effects on SICR behaviour in ESMs. Therefore, numerical simulations at different scales, such as mesoscale modelling [8, 9] and molecular dynamics simulations [10, 11], have been performed to investigate the shock compression response and SICR process of Al/Ni powder composites.

Powder composites and multi-layered composites are the two most common types of Al/Ni composites studied recently. Al/Ni powder composites are usually manufactured by powder compaction, including static pressing [12, 13] and explosive consolidation [14, 15], with various initial particle shapes (spherical, flaky and arbitrary) and different nanoscale/micron-scale particle sizes. Thus, the studies on Al/Ni powder composites are always related to the initial particle morphologies. Multi-layered composites are commonly manufactured via physical vapour deposition [16, 17] or cold rolling [18, 19], where the microstructure mainly depends on manufacturing and process methods. Vapour deposition for Al/Ni multi-layered composites, such as sputter deposition, can be used to precisely control layer thickness and to obtain a uniform multi-layered microstructure, which is a time-consuming and high-cost process. Cold rolling is a mechanical processing technique with repeatedly stacking and compressing initially alternated parallel Al and Ni foils to obtain the designed thickness. In general, the cold-rolled multi-layered composites contain nonuniform layer thicknesses. Kuk et al. [2] exploited a process combining deposition and cold rolling to reduce manufacturing costs, as well as to obtain uniform and continuous bilayers. In most studies on multi-layered composites, the bilayer spacing [17], in other words, the reactant spacing referring to the total thickness of the two layers, is an important parameter. Generally, the particle morphology and particle distribution in the microstructure of Al/Ni powder composites are totally different from that of Al/Ni multi-layered composites, which directly affect the shock response and SICR characteristics of this kind of materials.

Previous studies on energy-releasing aspect of Al/Ni multi-layered composites mainly focused on the self-propagating high-temperature synthesis (SHS) via differential scanning calorimetry (DSC) at a normal heating rate in the range of 20–40 °C min^{-1} [17, 20–22]. Knepper et al. [17] measured heat of reaction and reaction velocities of SHS in nonuniform reactants and characterized them as a function of the average bilayer spacing. As for the vapour-deposited multi-layered composites with layers in a nanoscale thickness, the diffusion distance and interface impurities in multi-layered composites were reduced, in comparison with the powder composites [5, 20]. Thus, the initial purpose of the study on Al/Ni multi-layered composites was to increase the reaction velocity and to enable self-propagating reactions in the materials. However, the fewer impurities also cause metastable intermetallic phases at the interface, which dominate the reaction velocity of the multi-layered composites with thin bilayers. The intermetallic layers have little effect on the reaction velocity of thicker bilayers, which is mainly controlled by the bilayer spacing and layer thickness [20].

Ji et al. [23] studied the SICR characteristics of Al/Ni multi-layered composites with 4 rolling passes via two-step impact initiation experiments and analysed the relationship between the released energy and the impact velocity. Kelly and Thadhani [16] investigated the shock compression response of Al/Ni multi-layered composites with 150 μm thickness by laser-driven flyer impact experiments. Comparing the high resolution transmission electron microscopy (TEM) characterization of the recovered unreacted specimens with that of the original specimens, they suggested chemical reactions are most likely to be initiated at pre-existing microstructural heterogeneities. The shock wave propagation in Al/Ni multi-layered composites is affected by the orientation of the material interfaces, the interfacial strength and the bilayer spacing, according to the mesoscale simulation by Specht et al. [18, 19]. These simulations

Journal : 10853 - Large 10853 Dispatch : 17-1-2019 Pages : 17
Article No. : 3357 LE TYPESET
MS Code : JMSC-D-18-08395 CP DISK

showed that the interfaces between Al and Ni layers would cause the dispersion and dissipation of the shock waves when the impact direction was parallel to them. In general, the SICR of Al/Ni composites are dominated by the microstructure of the composites and shock conditions. However, little is known about the energy release capacity and reaction mechanisms of Al/Ni multi-layered composites.

This work studied the SICR behaviour of Al/Ni composites by considering the manufacturing method. Different manufacturing methods, namely cold rolling with 3–5 passes and powder compaction, were used to obtain the Al/Ni composites. The stoichiometric ratios of different Al/Ni composites were kept in almost the same value. Two-step impact initiation experiments were performed to study the SICR behaviour of the Al/Ni composites at different impact velocities, where the energy release capacity was measured by the specific chemical energy e_r. Mesoscale simulations established based on the real microstructures were used to study the effects of the microstructure on the shock temperature in the Al/Ni composites. In order to reduce the interfacial effects on shock waves, initial thicknesses of Al and Ni foils were large enough ($\geq$ 0.5 mm) and the impact direction was perpendicular to the interfaces between Al and Ni layers. The inhibition effects of the interfacial intermetallic layers on the contact between Al and Ni layers were also studied in the mesoscale simulation. The simulation results made contributions to explain the different SICR behaviour in the experiments.

Methods

Sample preparation and microstructural characterization

The Al/Ni composites used in the present investigation were manufactured by using methods of cold rolling and powder compaction. The cold-rolled specimens were made of Al and Ni foils with an initial thickness of 0.8 mm and 0.5 mm, respectively. The stoichiometric ratio of Al to Ni in all the specimens was set to 1:1, in order to maximize energy release capability [24]. The initial Al and Ni foils were assembled alternately and rolled to obtain about 35% reduction in thickness. The rolled composites were annealed in an inert atmosphere at a temperature of 823 K to relieve residual stresses and prevent cracks. The annealing temperature below the melting point of Al (933 K) was set to avoid thermal ignition of Al/Ni [25]. This process is referred to as one rolling pass. The deformed sheet was cut into two pieces and stacked by repeating the above process. The Al/Ni multi-layered composites with 3–5 rolling passes were obtained to study their SICR behaviour. On the other hand, the powder compacted specimens were made by Al and Ni powders with an average particle size of 0.023 mm and 0.075 mm, respectively. The initial powders with the desired compositions were mixed using a blender. Then the powder mixture was pressed into the desired size at an approximate pressure of 850 MPa by static pressing. Table 1 gives the volumetric percentage (vol%) and stoichiometric percentage (n%) of each component, theoretical material densities (TMD), average actual material densities (AMD) and average TMD percentage (TMD%) of the four composites. Some deviations of the compositions in the cold-rolled Al/Ni composites were caused by the limitation of the processing technology on the initial foils, which are acceptable. It was shown that the average TMD% values of all the Al/Ni composites are within a narrow range from 92.0% to 94.2%.

The microstructures of energetic structural materials always play a crucial role in both the mechanical and the SICR behaviour. Under shock conditions, the microstructures could affect the deformation of particles, propagation of shock wave and distribution of shock temperature, which would finally control the SICR characteristics of the Al/Ni composites. The initial microstructures of the Al/Ni composites with cold-rolling passes from 3 to 5 were obtained by Scanning electron microscopy (SEM), as shown in Fig. 1a–c. The darker phase in the SEM images is Al, while the lighter one is Ni. With successive rolling passes, the Ni foils were fractured into small pieces and surrounded by continuous Al matrix. The Al/Ni multi-layered composites with 3–5 rolling passes showed the similar microstructure with parallel Al and Ni layers. On the other hand, the SEM image of the Al/Ni powder composites revealed a different microstructure, as shown in Fig. 1e. Because of the dendritic and agglomerated particle morphology of Ni, as shown in Fig. 1d, the Ni powders deformed plastically and became interconnected as a continuous phase in the powder composites. Al particles with spherical shapes, which occupied nearly 60%

Journal : 10853 - Large 10853 | Dispatch : 17-1-2019 | Pages : 17
Article No. : 3357 | LE | TYPESET
MS Code : JMSC-D-18-08395 | CP | DISK

Table 1 Material properties of the Al/Ni composites

Manufacture methods	Rolling passes	vol%		n%		TMD (g cm^{-3})	Average AMD (g cm^{-3})	Average TMD%
		Al	Ni	Al	Ni			
Cold rolling	3	61.5	38.5	52.2	47.8	5.13	4.83	94.2
	4	61.5	38.5	52.2	47.8	5.13	4.72	92.0
	5	61.5	38.5	52.2	47.8	5.13	4.81	93.8
Powder compaction	0	59.4	40.6	50.0	50.0	5.26	4.91	93.3

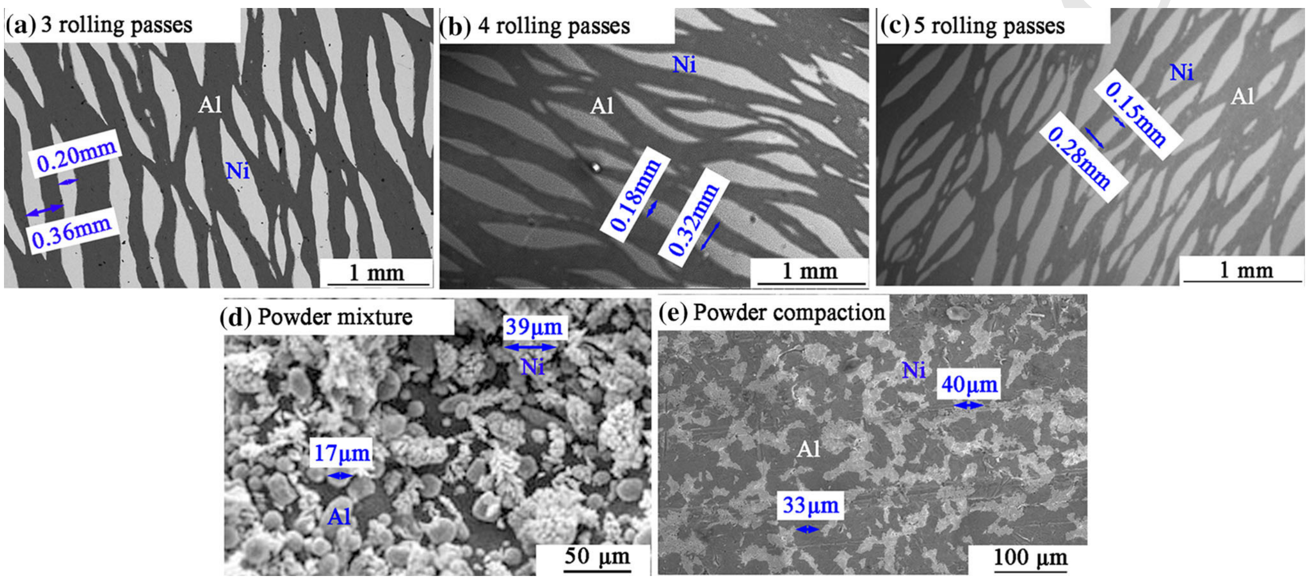

Figure 1 SEM photographs of the Al/Ni multi-layered composites with 3–5 rolling passes, Al/Ni powder mixture and the Al/Ni powder compaction.

volumetric fraction in the powder composites, also showed unapparent interfaces between each other. Typical layer thickness of Ni and the bilayer spacing were measured and are labelled in Fig. 1. Generally, the dimensions indicate that the thickness of the constituents was reduced during the rolling passes.

More SEM images of the Al/Ni composites with larger scales were obtained to observe the interfaces between Al and Ni layers in the microstructure, as shown in Fig. 2. Figure 2a–c shows that the third phase with different colours was produced at the interfaces of Al and Ni, which was determined by X-ray diffraction (XRD) as some intermetallics like Al_3Ni. This phenomenon indicates that mechanically induced atomic diffusion occurred at the interfaces. The intermetallic layers became thicker and more continuous with more rolling passes. Additionally, Fig. 2d reveals that no intermetallics were produced during the powder compaction process. The percentage of interfaces occupied by the intermetallics and the volumetric fraction of the intermetallics in Fig. 2 are listed in Table 2.

Experimental methods

Two-step impact initiation experiments, a typical method to investigate SICR characteristics of ESMs, were performed on the fragments of the Al/Ni composites manufactured differently. The experimental layout and the details of the experimental mechanism were described in our previous work [14, 26]. As shown in Fig. 3, the cylindrical Al/Ni fragments were fired by a 14.5-mm ballistic gun into a quasi-sealed test chamber with a volume of 35.2 litres, at a velocity in the range from 800 to 1500 m s^{-1}. During each experiment, the Al/Ni fragment experienced two impact processes: (a) The fragment perforated the thin target skin on the cover

Journal : 10853 - Large 10853 | Dispatch : 17-1-2019 | Pages : 17
Article No. : 3357 | □ LE | □ TYPESET
MS Code : JMSC-D-18-08395 | ✔ CP | ✔ DISK

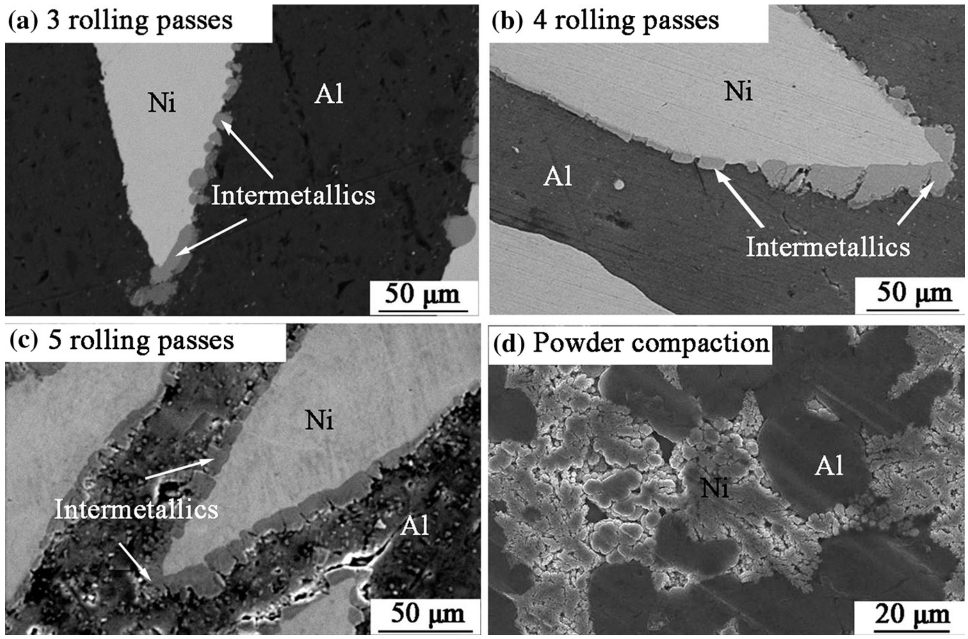

Figure 2 The SEM photograph showing the interfaces in the microstructures.

Table 2 Geometric information for intermetallics obtained from Fig. 2

Manufacture methods	Rolling passes	Occupying interfaces (%)	vol%
Cold rolling	3	45.6	3.5
	4	69.0	6.2
	5	100	11.8
Powder compaction	0	0	0

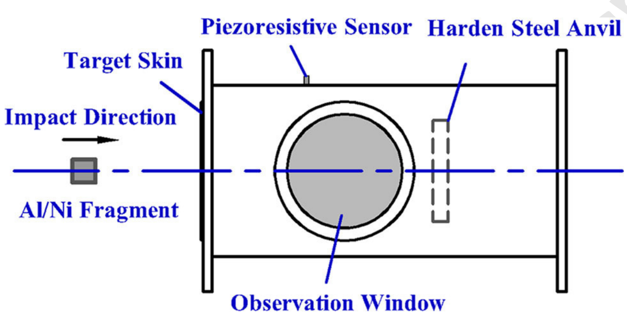

Figure 3 Schematic of two-step impact initiation experiments [26].

of the chamber; (b) The fragment impacted on the hardened steel anvil inside the chamber. Once the impact on the target interior reached the transition state, the Al/Ni fragments would react along with additional pressure and heat to the interior chamber. The launching direction of the fragments was perpendicular to the Al and Ni layers, which was assumed keeping the original direction during the impact process due to the guidance of sabots. The sabots were assumed to be totally separated from fragments before impacting on the chamber. A piezoresistive sensor was assembled in the chamber to measure the quasi-static pressure versus time (ΔP–t) curves. A high-speed camera was used to record the chemical reaction process images during the impact events. Clearly, both the manufacturing methods and the impact velocity are important factors to control the energy released by the Al/Ni composites, which finally determines the quasi-static pressure in the chamber.

Simulation details

Simulation model

In order to take further investigation on the influence of microstructure of the Al/Ni composites on their SICR behaviour, mesoscale simulations were conducted using ABAQUS/Explicit. The shock temperature and morphology evaluation of particles were focused from the simulation results. Because of the importance of particle configurations (size, shape and distribution) to shock response in the Al/Ni

Journal : 10853 - Large 10853 | Dispatch : 17-1-2019 | Pages : 17
Article No. : 3357 | ☐ LE | ☐ TYPESET
MS Code : JMSC-D-18-08395 | ☑ CP | ☑ DISK

composites, the mesoscale models were established based on the microstructure of the cross sections of the specimens obtained from SEM images (Fig. 1). The mesoscale modelling process is schematically shown in Fig. 4. The SEM image was vectorized firstly to obtain mathematical descriptions (such as points, lines and polygons). Then the vectorized image was imported to ABAQUS as a sketch file (Fig. 4c). Because of the size limitation of SEM images, the geometrical model was obtained by artificially extending the microstructure through mirroring/translation considering the periodicity of the microstructure. Additionally, the direction of the sketch was adjusted according to the actual manufacturing process and experimental setup to keep it perpendicular to the load direction (Fig. 4d).

According to Table 1, the four Al/Ni composites studied in this paper are highly dense composites with the TMD% in a narrow range from 92.0 to 94.2%. The voids are nearly invisible in the SEM images in Fig. 1 which can sufficiently reflect the microstructure in the composites. Although the SEM images with larger scales in Fig. 2 show some voids in the microstructures, they only reflect local area of the microstructure but could not reflect the distribution of particles and voids in the whole model. This paper concentrates on the influence of manufacturing methods on microstructures and finally on the shock response of Al/Ni composites. For simplification, more evidently different microstructural effects caused by different manufacturing methods, such as particle sizes and shapes were paid more attention in the mesoscale simulation. Therefore, the void effects are neglected in the simulation.

Eulerian-coupled temperature displacement eight-noded element (EC3D8RT) was used to simulate the shock response in the materials, where the ultrahigh strain rates would cause large deformations on materials. The thickness of the model equals the size of one element to simulate the 1-D process of shock wave propagating along the loading direction. Therefore, the proposed mesoscale model can be viewed as a slice of the real 3D microstructure. To decrease the cost of the 3D modelling, the computational model was implemented with a representative region which could sufficiently reflect the microstructure in the composites. As the result, the Euler domain was created with a size of 5 mm × 5 mm × 0.01 mm for the cold-rolled Al/Ni composites, where the optimized mesh size of 0.01 mm was used to ensure accurate calculation results with a reasonable CPU time. On the other hand, the smallest particle size in the Al/Ni powder composites was less than 20 μm. In order to describe the shock response in powder composites accurately, both the mesh size (0.002 mm) and the Euler domain (1 mm × 1 mm × 0.002 mm) should be much smaller. The four Al/Ni models were meshed with at least 10 elements across each particle, in order to keep the same accuracy when calculating the shock temperature in different materials. The Al and Ni materials were assigned to the Euler domain according to their location information and volume fraction. The mesoscale models are shown in Fig. 5.

Furthermore, as shown in Fig. 1, the intermetallic layers are nearly invisible in the SEM images with a reasonable magnification, which reflect the microstructure of the composites. Therefore, the size of the intermetallic layers can only be estimated from highly magnifying SEM images in Fig. 2. Here, our interest is mainly focused on the morphology evolution of the intermetallic layers during shock compression. A region of 1 mm × 1 mm × 0.001 mm of the cold-rolled Al/Ni composites with 3 passes was used as a standard region. The mesh size was set to

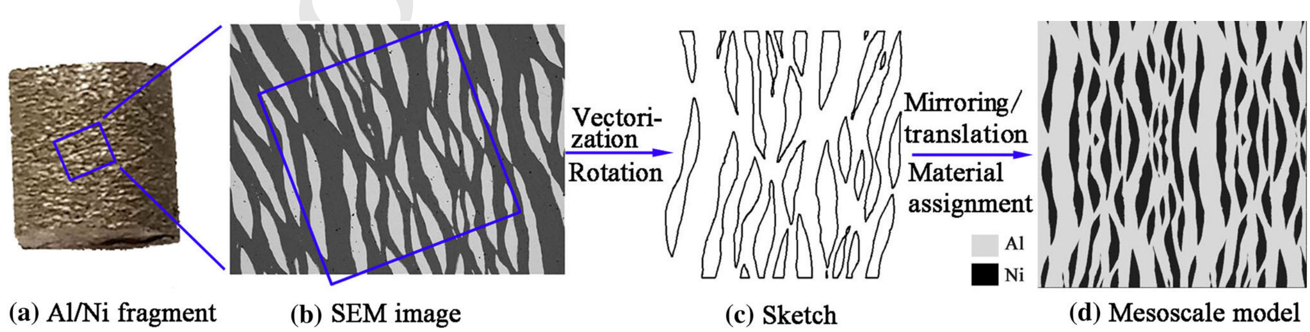

Figure 4 A schematic of the mesoscale modelling process.

Journal : 10853 - Large 10853 | Dispatch : 17-1-2019 | Pages : 17
Article No. : 3357 | ☐ LE | ☐ TYPESET
MS Code : JMSC-D-18-08395 | ☑ CP | ☑ DISK

Figure 5 Mesoscale models.

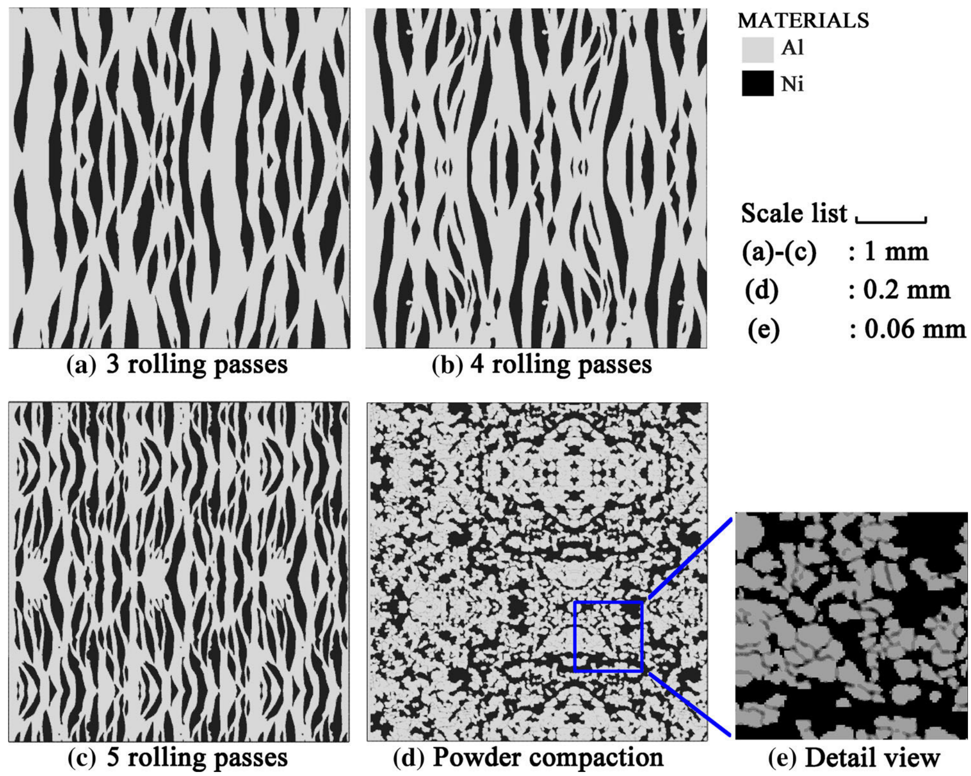

0.001 mm to keep at least 3 cells across each intermetallic layer.

Boundary conditions

A rigid plate was created on the left hand of the mesoscale model, with a velocity range from 300 to 1200 m s^{-1} to simulate the shock compression process. Hence, the particle velocity U_p in the Al/Ni composites equals the velocity of the plate. The mesh size of the rigid plate is the same as the Euler domain to prevent spurious reflections at the interface between the plate and Al/Ni due to large size changes of mesh. The both sides of the model along the thickness direction, as well as the upper and lower sides were prescribed with symmetric conditions to simulate a periodic microstructure and the 1-D shock compression process, as shown in Fig. 6.

Material model and parameters

Johnson–Cook (J–C) plasticity model [27], which is appropriate to describe the mechanical response of metals subjected to high strain rate loading and high temperature, was used to model the two components (Al and Ni). The J–C model is expressed as:

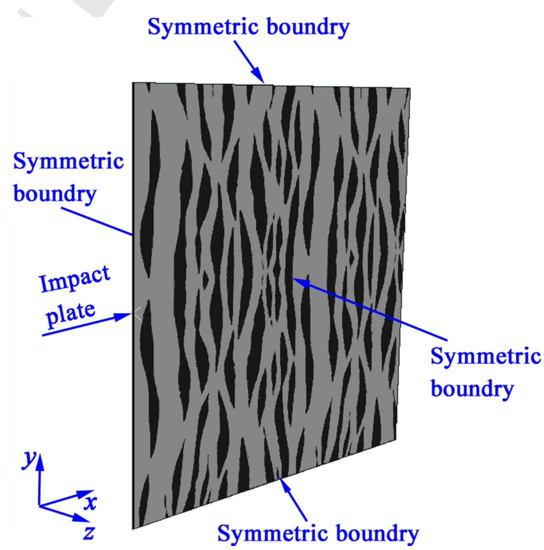

Figure 6 Boundary conditions.

$$\sigma_e = \left(A + B\varepsilon_e^n\right)\left(1 + C\ln\dot{\varepsilon}^*\right)\left(1 - T^{*m}\right) \quad (1)$$

Here, σ_e and ε_e are the equivalent stress and strain, respectively. $\dot{\varepsilon}^* = \dot{\varepsilon}_e/\dot{\varepsilon}_0$ is the dimensionless plastic strain rate and $\dot{\varepsilon}_0$ is a reference strain rate. $T^* = (T - T_{room})/(T_{melt} - T_{room})$ is the dimensionless temperature and T is the temperature. A is the yield strength under reference strain rate, which was

Journal : 10853 - Large 10853 Dispatch : 17-1-2019 Pages : 17
Article No. : 3357 □ LE □ TYPESET
MS Code : JMSC-D-18-08395 ✔ CP ✔ DISK

obtained by quasi-static tensile test on Al and Ni foils in this paper. B, n, C and m are material constants.

The Mie-Grüneisen equation of state (EOS) [28] was used to calculate the shock response of materials, which is defined in the form of:

$$P - P_H = \gamma\rho(E - E_H) \tag{2}$$

where P_H and E_H are the Hugoniot pressure and specific energy; γ is the Grüneisen coefficient; ρ is the density of materials.

The relationship between particle velocity (U_p) and shock velocity (U_s) is commonly described in a linear form of [29]:

$$U_s = C_0 + SU_p \tag{3}$$

where C_0 is the sound speed of materials; S is a material constant.

The simulations were conducted under adiabatic conditions; the temperature was contributed from plastic work dissipation. The evolution of temperature is defined as:

$$\dot{T} = \frac{\sigma : \dot{\varepsilon}}{\rho C_P} \tag{4}$$

Here, C_P is the specific heat capacity, σ is the stress, $\dot{\varepsilon}$ is the rate of plastic straining.

Defining G, λ as the shear modulus and thermal conductivity of the material, respectively, the material parameters for Al and Ni used in simulation are listed in Table 3. Due to lack of reference values of the mechanical and shock parameters of the intermetallic layers ($NiAl_3$), the mass average method was used for the qualitative analysis in this paper.

Table 3 Material parameters of Al and Ni

Material	Al	Ni	$NiAl_3$
ρ (kg m^{-3})	2784[a]	8875[a]	3368[d]
G (GPa)	26.2[b]	74.46[b]	46.47
A (MPa)	63	136	93.7
B (MPa)	200[c]	648[b]	388
n	0.3[c]	0.33[b]	0.31
m	0.5[c]	1.44[b]	0.89
C	0.01[c]	0.006[b]	0.008
T_{melt} (K)	933	1713	1261
C_p (J kg^{-1} K^{-1})	903[a]	444[a]	710
λ (W m^{-1} K^{-1})	237	90	175
C_0 (m s^{-1})	5370[a]	4590[a]	5042
S	1.29[a]	1.44[a]	1.35
γ	2.18[a]	2.00[a]	2.10

[a]Obtained from Refs. [26, 30]

[b]Obtained from Ref. [31]

[c]Obtained from Ref. [32]

[d]Obtained from Ref. [33]

Results and discussion

Experimental results and discussion

Experimental phenomenon of two-step impact initiation experiments

Figure 7 shows the SICR process of the Al/Ni multi-layered composites with 3 rolling passes at V = 841 m s^{-1} in the test chamber. As shown in Fig. 7a, the Al/Ni fragments firstly penetrated the thin target skin on the cover of the chamber. Then the Al/Ni fragments impacted the interior hardened steel anvil causing temperature rising in the material [26]. If chemical reaction occurred, two significant phenomena would be observed. On the one hand, the test chamber glowed strongly due to the Al/Ni fragments for several milliseconds and sometimes accompanied by chemical reaction products venting from the chamber, as shown in Fig. 7b, c. Gradually, the Al/Ni fragments finished its chemical reaction along with weaker flame (Fig. 7d, e). On the other hand, the pressure in the chamber was raised with the energy released from chemical reaction, which was monitored by the piezoresistive sensor, as shown in Fig. 8. The declined stage in the curves corresponds to the process that the leaking rate of the pressure from the hole on the target skin is higher than the chemical energy releasing rate in the chamber.

SICR behaviour of the Al/Ni composites with different manufacturing methods

The peak value of the quasi-static pressure ΔP_m can be used to calculate the energy deposition in the chamber, ΔQ, by the relationship below [34]:

$$\Delta P_m = (\gamma_a - 1)\Delta Q / V_E \tag{5}$$

where V_E is the volume of the test chamber, γ_a is the ratio of the specific heat of the gas in the chamber, which is assumed to be a constant of 1.4 as a standard value. This equation was derived by Ames [34] based

Journal : 10853 - Large 10853 | Dispatch : 17-1-2019 | Pages : 17
Article No. : 3357 | LE | TYPESET
MS Code : JMSC-D-18-08395 | CP | DISK

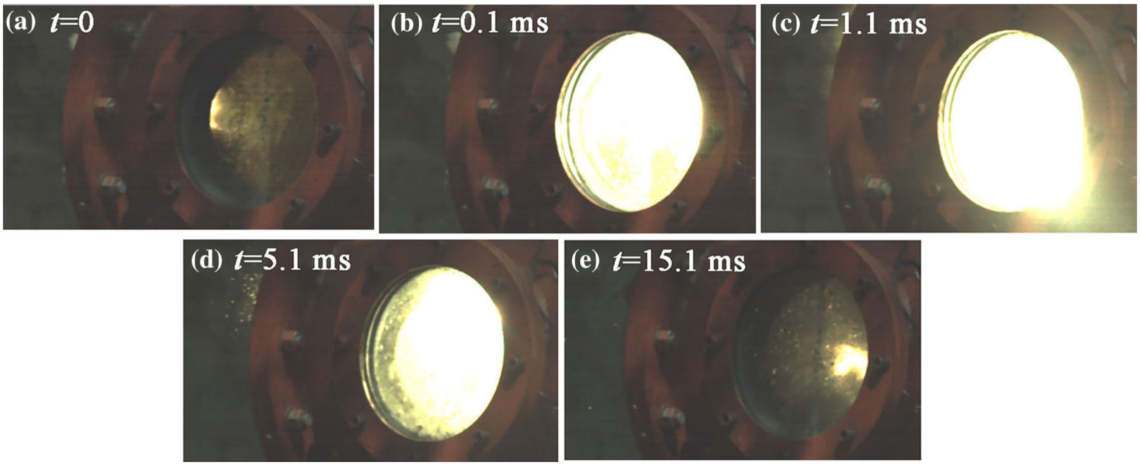

Figure 7 Typical photographs from high-speed camera of the SICR process in the test chamber.

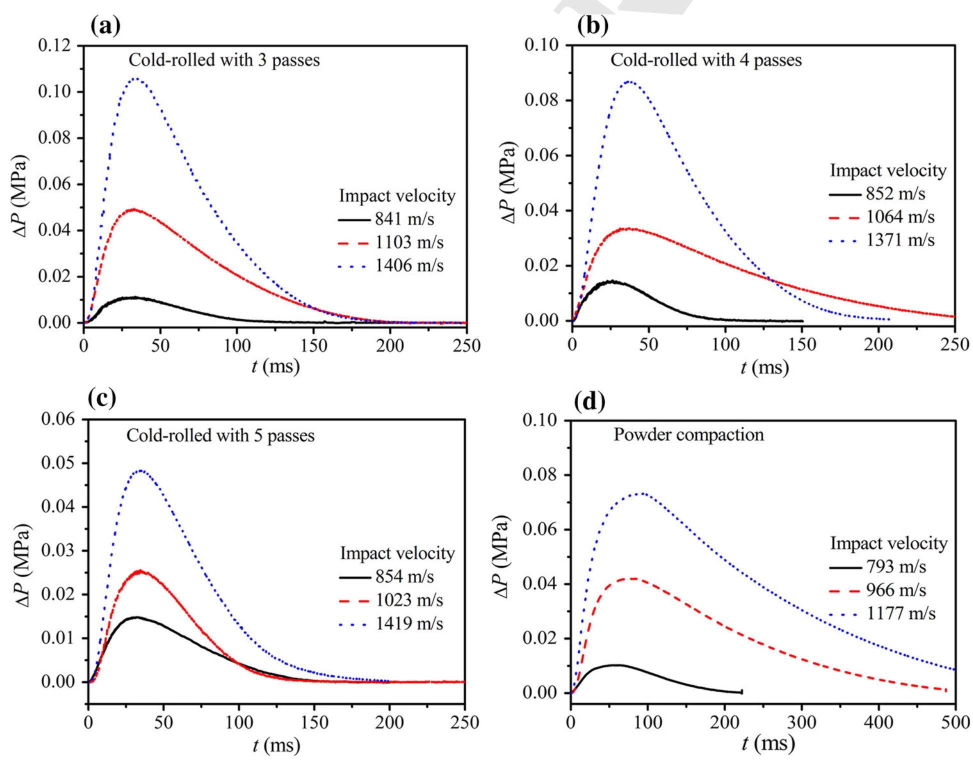

Figure 8 Typical quasi-static pressure versus time (ΔP–t) curves in two-step impact initiation experiments.

on the assumption that the test chamber was a closed system up to the point where the peak quasi-static pressure was obtained.

Between Al and Ni, the chemical reaction is complex as various potential reaction products would appear at different temperatures or shock conditions, as presented in Eq. (6):

$$\begin{aligned} &x\mathrm{Al} + y\mathrm{Ni} \rightarrow \mathrm{Al}_x\mathrm{Ni}_y \\ &4\mathrm{Al} + 3\mathrm{O}_2 \rightarrow 2\mathrm{Al}_2\mathrm{O}_3 \\ &2\mathrm{Ni} + \mathrm{O}_2 \rightarrow 2\mathrm{NiO} \end{aligned} \tag{6}$$

Assuming ΔQ only contains the residual kinetic energy of the fragments E_k and the energy released by chemical reaction E_r, one can define a specific chemical energy e_r to measure the chemical energy capacity of the Al/Ni composites:

$$e_r = E_r/m = (\Delta Q - E_k)/m \tag{7}$$

Here, e_r represents the chemical energy released by unit mass of Al/Ni composites, which eliminates the influence of mass and kinetic energy.

Most publications [23, 26, 34] related to the experiments all assumed fragments entered the test chamber at 80% or 90% of its kinetic energy, which neglected the effects of impact velocities, size of the fragments, as well as the materials and thickness of the steel skin. In order to reduce the errors from these effects, THOR equation [35] was adopted in this paper to calculate the residual kinetic energy:

$$V_r = V - 0.3048 \times 10^{c_1}(61023.75hA)^{c_2}(15432.1M)^{c_3}(3.28084V)^{c_4} \quad (8)$$

where h = 0.5 mm is the thickness of the target skin; A and M are the striking area and the mass of the fragments; c_1–c_4 are the constants related to the target materials. Equation (8) is applicable to spherical fragments and various target materials, including the mild steel used in the two-step initiation experiments. According to Ref. [35], the constants for a mild steel target were $c_1 = 6.399$, $c_2 = 0.889$, $c_3 = -0.945$, $c_4 = 0.019$.

Assuming the whole fragments impacted into the chamber, attaching with the target skin with the same striking area, the residual kinetic energy could be defined as:

$$E_k = \frac{1}{2}(m + m_t)V_r^2 \quad (9)$$

Here, m_t is the mass of the attaching target skin. The related parameters and calculated results of the two-step impact initiation experiments are presented in Table 4. It revealed that the residual kinetic energy was 74.5–91.9% of the original value.

According to Eqs. (5) and (7), the peak value of the quasi-static pressure in the chamber, ΔP_m, and the specific chemical energy released from the materials, e_r, are the two key parameters to weigh the energy release capability of the Al/Ni composites. Figure 9 depicts the relationships between the ΔP_m and e_r with the impact velocities for the four Al/Ni composites studied. The symbols represent the experimental points, while the curves are obtained by nonlinear fitting of the points. It should be noted that ΔP_m is related to both the residual kinetic energy and the released chemical energy, which increases with the impact velocity. Moreover, Fig. 9b shows a similar regularity with Fig. 9a, but the specific chemical energy tends to rise to a maximum value at high velocities once one of the reactants is depleted. When the impact velocity equals 1419 m s^{-1}, the e_r of the Al/Ni composites with 5 rolling passes almost reaches its peak value of 0.56 kJ g^{-1}. The target skins were all collected after experiments to judge whether the fragment broke up before or during the perforating process. Two typical target skins collected are shown in Fig. 10. The perforation by a complete fragment produced only one hole on the skin, while the broken up fragments produced several holes. As for the Al/Ni powder composites, the fragment broke up before perforating the target skin at 1303 m s^{-1} (Fig. 10b), which led to significant mass losses and the decrease in e_r. Additionally, our previous work [36] demonstrated that the chemical reaction only occurs when the impact velocity exceeds a critical value. From Fig. 9b, the critical velocities to initiate the chemical reaction in the Al/Ni powder composites and the multi-layered composites with 3 passes are approximately 793 m s^{-1} and 841 m s^{-1}, respectively. The impact velocity between the two critical values, which can initiate the SICR and cause completed reaction, respectively, leads to a partial chemical reaction of the Al/Ni composites.

As shown in Fig. 9b, the e_r–V curve of the powder compacted Al/Ni composites shows the highest energy release capability among the four composites by producing the highest e_r at the same impact velocity. It also appears that the energy release capability decreases with the growth of rolling passes. The e_r–V curve of the Al/Ni composites with 3 rolling passes in Fig. 9b was always higher than those of the other two cold-rolled composites and nearly approached its peak value at the velocity of 1406 m s^{-1}. On the other hand, the Al/Ni composites with 4 rolling passes presented a continuous up trend at this velocity.

Mesoscale simulation results and discussion

Effects of impact velocity on shock temperature at mesoscale

In order to investigate the influence of impact velocity on shock temperature, a typical particle morphology and the corresponding shock temperature profiles were obtained from mesoscale simulations of the Al/Ni multi-layered composites with 3

Journal : 10853 - Large 10853	Dispatch : 17-1-2019	Pages : 17
Article No. : 3357	□ LE	□ TYPESET
MS Code : JMSC-D-18-08395	✔ CP	✔ DISK

Table 4 Experimental parameters and calculated results

Manufacturing methods	Rolling passes	D (mm)	M (g)	V (m s^{-1})	ΔP_m (MPa)	ΔQ (KJ)	E_k (KJ)	e_r (KJ g^{-1})
Cold rolling	3	11.8	2.94	841	0.011	0.97	0.80	0.06
			2.98	872	0.016	1.41	0.89	0.17
			2.59	1103	0.049	4.31	1.31	1.16
			2.95	1382	0.081	7.13	2.55	1.55
			2.74	1406	0.105	9.24	2.44	2.48
	4	11.8	2.69	852	0.014	1.23	0.74	0.18
			2.59	1032	0.024	2.11	1.12	0.38
			2.67	1064	0.033	2.90	1.25	0.62
			2.79	1327	0.058	5.10	2.19	1.04
			2.73	1371	0.087	7.66	2.30	1.96
	5	12.8	2.98	854	0.015	1.32	0.81	0.17
			2.9	1023	0.025	2.20	1.21	0.34
			2.88	1049	0.028	2.46	1.28	0.41
			2.88	1419	0.048	4.22	2.60	0.56
Powder compaction	0	10	2.87	793	0.01	0.88	0.73	0.05
			2.88	939	0.026	2.29	1.08	0.42
			2.84	966	0.042	3.70	1.13	0.90
			2.89	1177	0.073	6.42	1.80	1.60
			2.87	1303	0.068	5.98	2.24	1.30

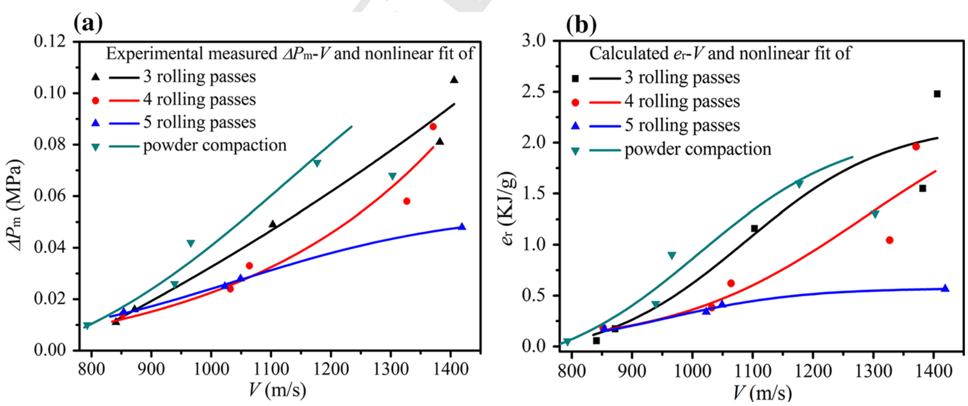

Figure 9 Two important relationships for the four Al/Ni composites: **a** the peak value of quasi-static pressure and the impact velocity (ΔP_m–V); **b** the specific chemical energy and the impact velocity (e_r–V).

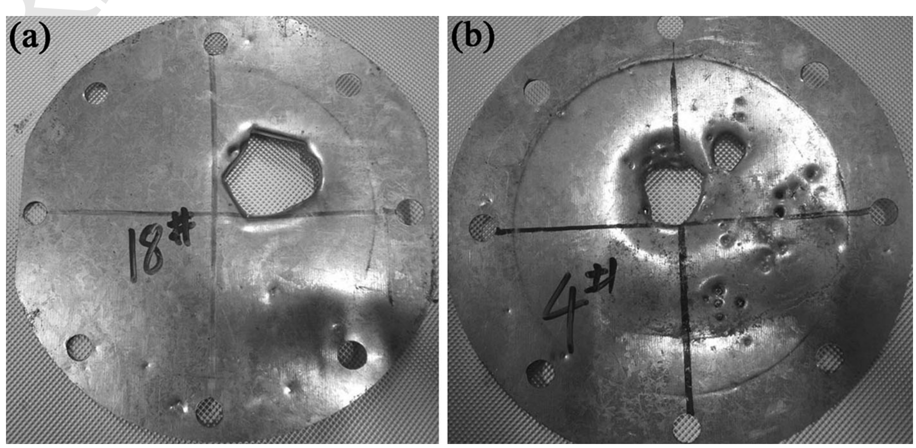

Figure 10 Two typical target skins after penetration of fragments which **a** kept complete and **b** broke up during the experiment.

Journal : 10853 - Large 10853 | Dispatch : 17-1-2019 | Pages : 17
Article No. : 3357 | ☐ LE | ☐ TYPESET
MS Code : JMSC-D-18-08395 | ☑ CP | ☑ DISK

rolling passes at an impact velocity of 300, 800 and 1200 m s^{-1}, respectively, as shown in Fig. 11. All the profiles are selected when the shock waves arrive at the same position. It is worth noting that the Euler simulation was established without consideration of any fracture of materials. It appears that the temperature increases with the propagation of shock waves, as a result of the rapid plastic deformations of each layer and the volume change of the composites. Al exhibited the higher temperatures than Ni due to more compressibility. The simulation results indicate that the increase on impact velocity causes large deformations and high shock temperatures in the composites.

Assuming the SICR process is controlled by shock temperature, partial reaction takes place when shock temperature reaches a critical value on initiation of SICR [26, 37]. Higher impact velocity causes higher shock temperature in the composites and finally leads to a growing trend of the reaction efficiency. Therefore, the Al/Ni composites release more chemical energy at high impact velocities before complete reaction. This explains the increasing trend of e_r with impact velocities in the partial reaction range in the experimental results.

Microstructure effects on shock temperature of the Al/Ni composites

The shock temperature profiles under U_{p} = 1200 m s^{-1} are shown in Fig. 12, corresponding to the simulation results of the Al/Ni composites with gradually decreased particle size. Since Al/Ni composites are commonly heterogeneous materials, chemical reactions are most likely to be locally initiated. The highest temperature areas were analysed as the most potential initiation sites where chemical reactions likely occur. From Fig. 12a–d, it can be seen that the Al/Ni composites with large particle size produced more highly elevated temperature spots. This phenomenon is in consistent with Specht's simulation results [19], which are related to the Al/Ni multi-layered composites under the shock front parallel to the laminate layers. The shock waves would reflect at the interface due to the impedance difference between Al and Ni, which resulted in increase in interfacial strains and temperatures in materials. With decreasing the particle size, the Al/Ni system reached an equilibrating state quickly and the temperature distribution became uniform with less highly elevated temperature spots.

With propagation of shock waves, the temperature rises from two branches, i.e. (1) one branch is the rapid deformations of each layer and the volume change of the composites at the shock pressure; (2) the second branch is the heat transfer between each

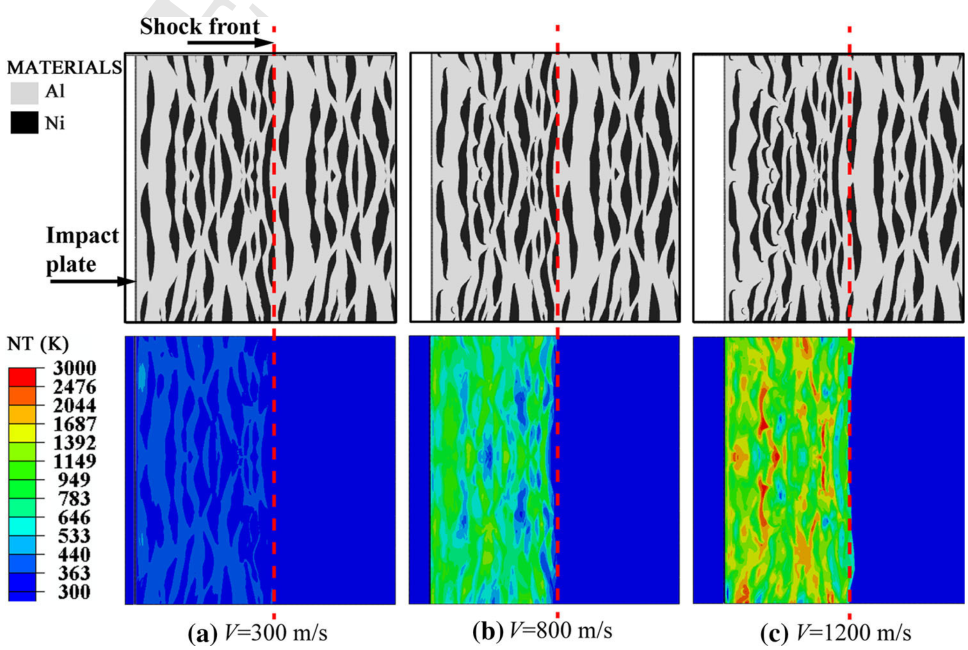

Figure 11 A typical particle morphology and the corresponding shock temperature profiles of Al/Ni composites with 3 rolling passes at different impact velocities.

Journal : 10853 - Large 10853 | Dispatch : 17-1-2019 | Pages : 17
Article No. : 3357 | ☐ LE | ☐ TYPESET
MS Code : JMSC-D-18-08395 | ☑ CP | ☑ DISK

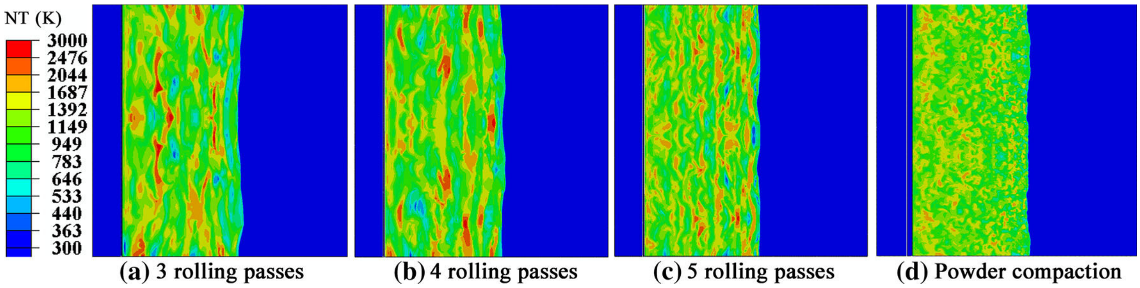

Figure 12 Typical shock temperature profiles for the Al/Ni composites with U_p = 1200 m s^{-1}.

layer. According to the research [25], the thermal ignition temperature of Al/Ni is close to the melting point of Al (933 K). It also should be noted that the recent research revealed that thermal or mechanical stimuli could decrease the ignition temperature for chemical reaction [6, 38]. In order to provide an overall qualitative analysis on the SICR potency of each Al/Ni composite from the point of view of thermal ignition, effective temperature areas above 933 K were visualized by a red spectrum, as shown in Fig. 13. It appears that a decrease of particle size leaded to a monotonic increase of effective ignition temperature area, which means the heat transfer velocity increased with the decrease of particle size. The Al/Ni powder compositions distinctly revealed the most uniformed and largest effective temperature distribution, due to its nearly one-tenth particle size of the multi-layered composites.

Morphology evolution of intermetallics during shock compression

Since Fig. 2 shows much localized microstructures, the information in Table 2 could not represent the distribution of the intermetallics in the whole microstructure. However, it could be speculated that the energy released from the Al/Ni multi-layered composites with 3–5 passes would be decreased by 3.5, 6.2 and 11.8%, respectively, due to the decrease of the reactants. Besides, the intermetallic layers inhibited the contact between Al and Ni layers, which would also affect the energy release capability of the Al/Ni composites.

Two typical average thickness ratios δ (64 and 24) of Ni layer to intermetallic layer, which are, respectively, corresponding to the Al/Ni composites with 3 rolling passes and 5 rolling passes, were chosen to study their inhibition effects on the contact between Al and Ni layers. The geometric outline of the intermetallic layer was implemented by scaling the outline of each Ni layer from the centroid with the corresponding ratio of $(1 + 2/\delta)$. Material volume fraction in elements, commonly abbreviated to EVF, can clearly reflect both the morphology and the content of each component. The EVF profiles of intermetallic layers for the models with the two δ ratios are shown in Fig. 14. Due to the irregular shape of the Ni layers, the intermetallic layers produced by the scaling method revealed a nonuniform distribution, which corresponds to the real nonuniform and discontinuous microstructures in SEM images.

It is clear that the intermetallic layers deformed severely during shock compression. With plastic flow and local accumulation of the intermixing materials, breakage occurred or expanded at the thin area, especially in the Al/Ni composites with relatively

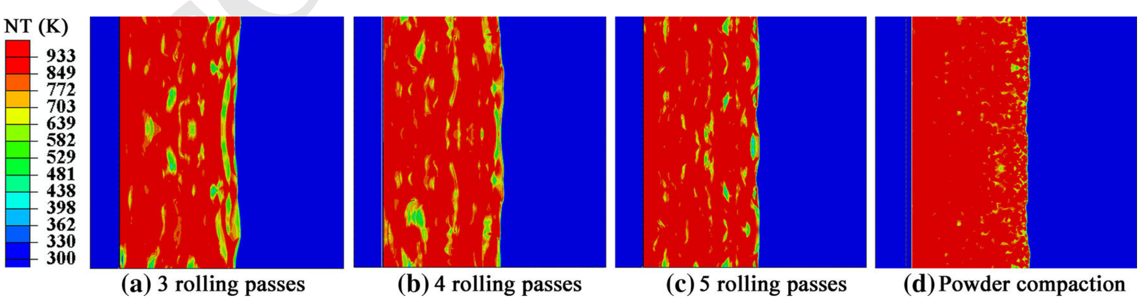

Figure 13 Effective ignition temperature profiles for the four Al/Ni composites.

Journal : 10853 - Large 10853 | Dispatch : 17-1-2019 | Pages : 17
Article No. : 3357 | ☐ LE | ☐ TYPESET
MS Code : JMSC-D-18-08395 | ☑ CP | ☑ DISK

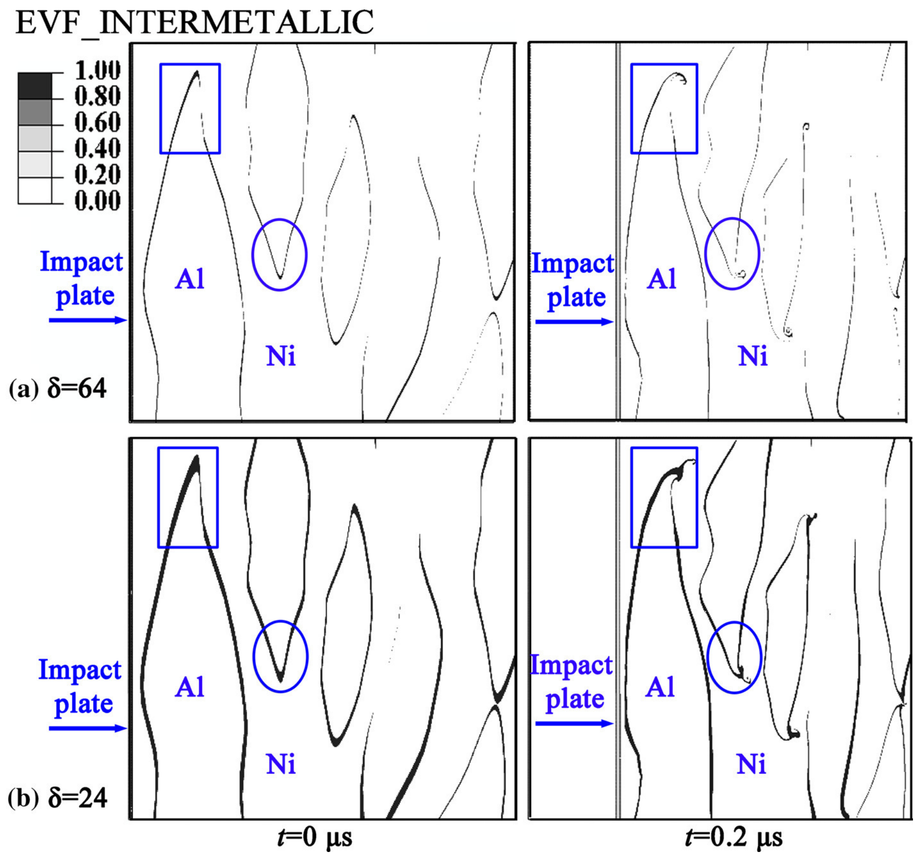

Figure 14 The morphology evolution of the intermetallic layers with two designed thickness during shock compression with U_p = 1200 m s^{-1}.

large δ. As the result, Al and Ni layers came into contact at the breakage area and would react when reached initiation conditions. On the other hand, the remaining interfacial Al–Ni intermetallic layers continued hinder the contact between Al and Ni, which would finally affect the reaction efficiency of Al/Ni composites.

Microstructure effects on SICR behaviour of the Al/Ni composites

Based on the above analysis, we can make further explanation on the influence of microstructure on SICR behaviour. As for the Al/Ni powder composites, there are no intermetallics existing between the two components, where Al and Ni particles are fully contacted. Assuming the mechanism of SICR is similar to thermal ignition, which means chemical reaction occurs once temperature reaches the melting point of Al. It could be seen that the Al/Ni powder composites produced a significantly larger effective ignition temperature area than the mulit-layered composites from the simulation results. This means the largest amount of reactants in the Al/Ni powder composites were initiated at the same shock conditions. Therefore, the Al/Ni powder composites showed the highest energy release capability among the four composites in the two-step impact initiation experiments.

Regarding to the Al/Ni multi-layered composites, the effective ignition temperature area increased with the growth of rolling passes. However, from the two-step impact initiation experimental results, e_r showed a contrary regularity that decreased with the rolling passes. This leads to the conclusion that the effective ignition temperature area is not the only factor which controls the SICR characteristics. From the simulation results, the highly elevated temperature spots decreased with the growth of rolling passes, which resulted in a decrease of the most potential initiation sites. Additionally, the simulation results revealed the intermetallic layers at the interface of the cold-rolled Al/Ni composites immediately prevented the contact between reactants (Al and Ni), which would be locally broken up at the thin areas during shock compression. Therefore, the e_r of the Al/Ni composites with 4 rolling passes shown in Fig. 9b would reach its peak value at the higher velocity than the

Journal : 10853 - Large 10853 | Dispatch : 17-1-2019 | Pages : 17
Article No. : 3357 | LE | TYPESET
MS Code : JMSC-D-18-08395 | CP | DISK

composites with 3 rolling passes. However, thicker intermetallic layers in the Al/Ni multi-layered composites would keep hindering the contacts between Al and Ni due to low breakages. Especially for the composites with 5 cold-rolling passes, the intermetallic layers was produced at almost all the interfaces which finally affected the energy release capacity of the composites. These two factors, namely highly elevated temperature spots and intermetallic layers, caused by the microstructural difference, could be used to explain the SICR characteristic difference among the three Al/Ni multi-layered composites.

Conclusions

The study shows that different manufacturing methods can be used to control the microstructure of Al/Ni composites which can then influence the SICR behaviour. The research work gives a better understanding on SICR behaviour of Al/Ni composites by two-step impact initiation experiments on Al/Ni multi-layered composites manufactured by cold rolling with 3–5 passes and Al/Ni powder composites. Furthermore, two main factors, namely distribution of shock temperature and the morphology evolution of the interfacial intermetallic, have been analysed to study their contribution and inhibition to the SICR characteristics. Based on the research carried out, the following conclusions can be drawn:

1. The SEM images have clearly revealed different microstructures between the Al/Ni multi-layered composites and the Al/Ni powder composites. In the Al/Ni multi-layered composites, the Ni foils are fractured into pieces and surrounded by continuous Al matrix. Besides, intermetallic phase has also been observed at the interfaces between Al and Ni. The layer thicknesses of the constituents are reduced during the rolling passes, while the content of the interfacial intermetallic shows an increasing tendency. The microstructure of the Al/Ni powder composites, of which the particle size is one-tenth of the multi-layered composites, showed no intermetallic at the interfaces.
2. From the point of view of thermal ignition, temperature area above the melting point of Al (933 K) is obtained to reflect the overall SICR potency of the Al/Ni composites from mesoscale simulation. It appears that the Al/Ni powder composites with relatively smaller particle size produce significantly large effective ignition temperature area. Therefore, the powder composition has the highest energy release capability among the four composites by producing the highest specific chemical energy e_r at the same impact velocity.
3. The highly elevated temperature spots, which reflect the most potential initiation sites, decrease with more cold-rolling passes. Also, the multi-layered composites with thick and large contents of intermetallics show less breakages during shock compression. As the result, the energy release capability of the Al/Ni multi-layered composites decreases with the growth of rolling passes in the experimental results.

Generally, the SICR of Al/Ni composites is a complicated process, which is controlled by both the temperature distribution (including the effective ignition temperature area and highly elevated temperature spots) and the morphology of intermetallic layers. Understanding the influence of microstructure on the SICR behaviour of Al/Ni composites is an essential step to design such materials and exploit further advantages for a wide variety of applications.

Acknowledgements

This research is supported by the National Program for Support of Top-notch Young Professionals of China, the Fundamental Research Funds for the Central Universities (No. 30916011305) and China Scholarship Council. The authors would also like to thank Mr. Jiajie Deng, Mr. Fei Gao, Mr. Chuang Liu, Mr. Chenyang Xu, Mr. Wenjie Wang, Miss Mengting Tan and Miss Xue Wu for their great support on the current experimental work.

References

[1] Song I, Thadhani NN (1992) Shock-induced chemical reactions and synthesis of nickel aluminides. Metall Mater Trans A 23(1):41–48. https://doi.org/10.1007/BF02660849

[2] Kuk SW, Ryu HJ, Yu J (2014) Effects of the Al/Ni ratio on the reactions in the compression-bonded Ni-sputtered Al foil

Journal : 10853 - Large 10853 | Dispatch : 17-1-2019 | Pages : 17
Article No. : 3357 | ☐ LE | ☐ TYPESET
MS Code : JMSC-D-18-08395 | ☑ CP | ☑ DISK

multilayer. J Alloys Compd 589:455–461. https://doi.org/10.1016/j.jallcom.2013.12.020

[3] Baker EL, Daniels AS, Ng KW, Martin VO, Orosz JP (2001) Barnie: a unitary demolition warhead. Paper presented at the 19th International Symposium on Ballistics Interlaken, Switzerland

[4] Nielson DB, Ashcroft BN, Doll DW (2013) Reactive material compositions and projectiles containing same.. U.S. patent 8,568,541

[5] Hugus GD, Sheridan EW, Brooks GW (2012) Structural metallic binders for reactive fragmentation weapons. U.S. patent 8,250,985

[6] Reeves RV, Mukasyan AS, Son SF (2010) Thermal and impact reaction initiation in Ni/Al heterogeneous reactive systems. J Phys Chem C 114(35):14772–14780

[7] Herbold EB, Thadhani NN, Jordan JL (2011) Observation of a minimum reaction initiation threshold in ball-milled Ni + Al under high-rate mechanical loading. J Appl Phys 109(6):066108

[8] Qiao L, Zhang XF, He Y, Zhao XN, Guan ZW (2013) Multiscale modelling on the shock-induced chemical reactions of multifunctional energetic structural materials. J Appl Phys 113(17):173513. https://doi.org/10.1063/1.4803712

[9] Eakins DE, Thadhani NN (2008) Mesoscale simulation of the configuration-dependent shock-compression response of Ni + Al powder mixtures. Acta Mater 56(7):1496–1510

[10] Cherukara MJ, Germann TC, Kober EM, Strachan A (2016) Shock loading of granular Ni/Al composites. Part 2: shock-induced chemistry. J Phys Chem C 120(12):6804–6813

[11] Cherukara MJ, Germann TC, Kober EM, Strachan A (2014) Shock loading of granular Ni/Al composites. Part 1: mechanics of loading. J Phys Chem C 118(45):26377–26386. https://doi.org/10.1021/jp507795w

[12] Martin M (2005) Processing and characterization of energetic and structural behavior of nickel aluminum with polymer binders. Georgia Institute of Technology

[13] Zhang XF, Shi AS, Qiao L, Zhang J, Zhang YG, Guan ZW (2013) Experimental study on impact-initiated characters of multifunctional energetic structural materials. J Appl Phys 113(8):083508. https://doi.org/10.1063/1.4793281

[14] Wei CT, Vitali E, Jiang F, Du SW, Benson DJ, Vecchio KS, Thadhani NN, Meyers MA (2012) Quasi-static and dynamic response of explosively consolidated metal–aluminum powder mixtures. Acta Mater 60(3):1418–1432. https://doi.org/10.1016/j.actamat.2011.10.027

[15] Aydelotte BB, Thadhani NN (2013) Mechanistic aspects of impact initiated reactions in explosively consolidated metal + aluminum powder mixtures. Mater Sci Eng, A 570:164–171. https://doi.org/10.1016/j.msea.2013.01.054

[16] Kelly SC, Thadhani NN (2016) Shock compression response of highly reactive Ni + Al multilayered thin foils. J Appl Phys 119(9):095903. https://doi.org/10.1063/1.4942931

[17] Knepper R, Snyder MR, Fritz G, Fisher K, Knio OM, Weihs TP (2009) Effect of varying bilayer spacing distribution on reaction heat and velocity in reactive Al/Ni multilayers. J Appl Phys 105(8):083504. https://doi.org/10.1063/1.3087490

[18] Specht PE, Thadhani NN, Weihs TP (2012) Configurational effects on shock wave propagation in Ni–Al multilayer composites. J Appl Phys 111(7):073527. https://doi.org/10.1063/1.3702867

[19] Specht PE, Weihs TP, Thadhani NN (2016) Interfacial effects on the dispersion and dissipation of shock waves in Ni/Al multilayer composites. J Dyn Behav Mater 2(4):500–510. https://doi.org/10.1007/s40870-016-0084-0

[20] Gavens AJ, Van Heerden D, Mann AB, Reiss ME, Weihs TP (2000) Effect of intermixing on self-propagating exothermic reactions in Al/Ni nanolaminate foils. J Appl Phys 87(3):1255–1263. https://doi.org/10.1063/1.372005

[21] Ma E, Thompson CV, Clevenger LA, Tu KN (1990) Self-propagating explosive reactions in Al/Ni multilayer thin films. Appl Phys Lett 57(12):1262–1264. https://doi.org/10.1063/1.103504

[22] Kuk SW, Yu J, Ryu HJ (2015) Effects of interfacial Al oxide layers: control of reaction behavior in micrometer-scale Al/Ni multilayers. Mater Design 84:372–377. https://doi.org/10.1016/j.matdes.2015.06.173

[23] Ji C, He Y, Wang CT, He Y, Pan X, Jiao J, Guo L (2017) Investigation on shock-induced reaction characteristics of an Al/Ni composite processed via accumulative roll-bonding. Mater Design 116:591–598

[24] Dunbar E, Thadhani NN (1993) High-pressure shock activation and mixing of nickel–aluminum powder mixtures. J Mater Sci 28:2903–2914. https://doi.org/10.1007/BF00354693

[25] Thiers L, Mukasyan AS, Varma A (2002) Thermal explosion in Ni–Al system: influence of reaction medium microstructure. Combust Flame 131(1):198–209. https://doi.org/10.1016/S0010-2180(02)00402-9

[26] Xiong W, Zhang X, Tan M, Liu C, Wu X (2016) The energy release characteristics of shock-induced chemical reaction of Al/Ni composites. J Phys Chem C 120(43):24551–24559. https://doi.org/10.1021/acs.jpcc.6b06530

[27] Johnson GR, Cook WH (1983) A constitutive model and data for metals subjected to large strains, high strain rates and high temperatures. In: Proceedings of the 7th international symposium on ballistics. The Hague, pp 541–547

Journal : 10853 - Large 10853 | Dispatch : 17-1-2019 | Pages : 17
Article No. : 3357 | LE | TYPESET
MS Code : JMSC-D-18-08395 | CP | DISK

[28] Lemons DS, Lund CM (1999) Thermodynamics of high temperature, Mie–Gruneisen solids. Am J Phys 67(12):1105–1108. https://doi.org/10.1119/1.19091

[29] Meyers MA (1994) Dynamic behavior of materials. Wiley, New York

[30] Tang W, Zhang R (2008) Introduction to theory and computation of equation of state. Higher Education Press, Beijing

[31] Vitali E, Wei CT, Benson DJ, Meyers MA (2011) Effects of geometry and intermetallic bonding on the mechanical response, spalling and fragmentation of Ni–Al laminates. Acta Mater 59(15):5869–5880. https://doi.org/10.1016/j.actamat.2011.05.047

[32] Peyre P, Chaieb I, Braham C (2007) FEM calculation of residual stresses induced by laser shock processing in stainless steels. Model Simul Mater Sci 15(3):205–221. https://doi.org/10.1088/0965-0393/15/3/002

[33] Reding DJ (2010) Multiscale chemical reactions in reactive powder metal mixtures during shock compression. J Appl Phys 108:024905. https://doi.org/10.1063/1.3455850

[34] Ames RG (2005) Vented chamber calorimetry for impact-initiated energetic materials. Paper presented at the 43rd AIAA Aerospace Sciences Meeting and Exhibit, Reno, Nevada

[35] Lynch DD, Kunkel RW, Juarascio SS (1997) An analysis comparison using the vulnerability analysis for surface targets (VAST) computer code and the computation of vulnerable area and repair time (COVART III) computer code. Army Research Lab, Adelphi

[36] Xiong W, Zhang XF, Wu Y, He Y, Wang CT, Guo L (2015) Influence of additives on microstructures, mechanical properties and shock-induced reaction characteristics of Al/Ni composites. J Alloys Compd 648:540–549. https://doi.org/10.1016/j.jallcom.2015.07.004

[37] Boslough MB (1990) A thermochemical model for shock-induced reactions (heat detonations) in solids. J Chem Phys 92(3):1839–1848. https://doi.org/10.1063/1.458066

[38] White JDE, Reeves RV, Son SF, Mukasyan AS (2009) Thermal explosion in Al–Ni system influence of mechanical activation. J Phys Chem A 113:13541–13547

Journal : **10853 - Large 10853**	Dispatch : **17-1-2019**	Pages : **17**
Article No. : **3357**	☐ LE	☐ TYPESET
MS Code : **JMSC-D-18-08395**	☑ CP	☑ DISK

Journal : **10853**
Article : **3357**

Author Query Form

Please ensure you fill out your response to the queries raised below and return this form along with your corrections

Dear Author

During the process of typesetting your article, the following queries have arisen. Please check your typeset proof carefully against the queries listed below and mark the necessary changes either directly on the proof/online grid or in the 'Author's response' area provided below

Query	Details Required	Author's Response
AQ1	As per instruction page range must for this journal. Hence, please provide last page for reference [7, 8, 13, 16, 17, 18, 33].	
AQ2	Please provide complete details for reference [12], if available.	